BJR

https://doi.org/10.1259/bjr.20220980

Received: 19 October 2022 | Revised: 31 January 2023 | Accepted: 06 February 2023 | Published online: 06 March 2023

Cite this article as:
Savaridas SL, Agrawal U, Fagbamigbe AF, Tennant SL, McCowan C. Radiomic analysis in contrast-enhanced mammography using a multivendor data set: accuracy of models according to segmentation techniques. *Br J Radiol* (2023) 10.1259/bjr.20220980.

FULL PAPER

Radiomic analysis in contrast-enhanced mammography using a multivendor data set: accuracy of models according to segmentation techniques

[1,2]SARAH L SAVARIDAS, MBChB, FRCR, MD, [3]UTKARSH AGRAWAL, BE(Hons), MTech(Hons), PhD, [4,5]ADENIYI FRANCIS FAGBAMIGBE, BSc(Hons), MSc(Hons), PhD, MA, MPH, [6]SARAH L TENNANT, BMedSci, BMBS, MRCP, FRCR and [3]COLIN MCCOWAN, BSc(Hons), MSc, MSc, PhD

[1]School of Medicine, University of Dundee, Dundee, Scotland
[2]Ninewells Hospital, NHS Tayside, Dundee, United Kingdom
[3]School of Medicine, University of St. Andrews, St. Andrews, Scotland
[4]Department of Epidemiology and Medical Statistics, University of Ibadan, Ibadan, Nigeria
[5]Institute of Applied Health Sciences, University of Aberdeen, Aberdeen, United Kingdom
[6]Nottingham Breast Institute, Nottingham University Hospitals NHS Trust, Nottingham, England

Address correspondence to: Dr Sarah L Savaridas
E-mail: *ssavaridas@dundee.ac.uk*

Objective: Radiomic analysis of contrast-enhanced mammographic (CEM) images is an emerging field. The aims of this study were to build classification models to distinguish benign and malignant lesions using a multivendor data set and compare segmentation techniques.

Methods: CEM images were acquired using Hologic and GE equipment. Textural features were extracted using MaZda analysis software. Lesions were segmented with freehand region of interest (ROI) and ellipsoid_ROI. Benign/Malignant classification models were built using extracted textural features. Subset analysis according to ROI and mammographic view was performed.

Results: 269 enhancing mass lesions (238 patients) were included. Oversampling mitigated benign/malignant imbalance. Diagnostic accuracy of all models was high (>0.9). Segmentation with ellipsoid_ROI produced a more accurate model than with FH_ROI, accuracy:0.947 *vs* 0.914, AUC:0.974 *vs* 0.86, $p < 0.05$. Regarding mammographic view all models were highly accurate (0.947–0.955) with no difference in AUC (0.985–0.987). The CC-view model had the greatest specificity:0.962, the MLO-view and CC + MLO view models had higher sensitivity:0.954, $p < 0.05$.

Conclusions: Accurate radiomics models can be built using a real-life multivendor data set segmentation with ellipsoid-ROI produces the highest level of accuracy. The marginal increase in accuracy using both mammographic views, may not justify the increased workload.

Advances in knowledge: Radiomic modelling can be successfully applied to a multivendor CEM data set, ellipsoid_ROI is an accurate segmentation technique and it may be unnecessary to segment both CEM views. These results will help further developments aimed at producing a widely accessible radiomics model for clinical use.

BACKGROUND

Contrast-enhanced mammography (CEM) is a functional imaging technique, which utilises a dual-energy subtraction method following administration of intravenous contrast agent to produce 2D images demonstrating lesion vascularity.[1] During each breast compression two images—a low kV image and a high kV image—are acquired. As the low-energy (LE) image is below the k-edge of iodine, the image produced is equivalent to a standard mammographic view. Using digital post-processing the LE image is then subtracted from the high-energy image to produce a recombined (RC) image which demonstrates only the areas of enhancement. Thus, the RC image demonstrates the vascularity of breast lesions.

Textural analysis is a radiomics technique that evaluates the appearance, position and pattern of pixels according to their grey-level intensity within a digital image.[2,3] This allows quantitative analysis of medical images and has been shown to improve discrimination between benign and malignant lesions when applied to breast MRI. Measures of entropy and heterogeneity have particular merit as discriminatory factors as malignant lesions tend to demonstrate greater complexity.[4–6] Emerging evidence suggests textural analysis can also be applied to CEM images.[7–13] However,

Figure 1. CEM study of left breast, CC position. a: low-energy image, b: high-energy image, c: recombined image. CC, craniocaudal; CEM, contrast-enhanced mammography.

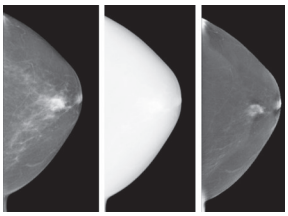

individual study numbers are small and research to date has been restricted to single site, single vendor CEM image data sets which then limits the findings generaliseability.[14] Furthermore, there is a dearth of evidence regarding the best technique for segmentation— whether it is necessary to segment an exact region of interest (ROI) outlining the lesion or whether more time-efficient techniques such as an ellipsoid ROI produce similar results. Finally, the majority of prior studies require segmentation of both LE images and RC images, often using both views.[7–11,13] There is little evidence for the efficacy of modelling based on RC features only.

As CEM becomes more widespread in clinical practice, it may offer an alternative to MRI in certain clinical settings. However, recent evidence indicates that whilst CEM has a higher specificity, MRI remains the more sensitive technique.[15] Quantitative assessment of CEM images, derived from textural feature modelling has the potential to improve diagnostic accuracy of CEM with extensive clinical implications. This novel study paves the way for a 'real-world' tool, with the aims to investigate the accuracy of a radiomics model that can be applied to textural features derived from a multivendor data set of RC images. We compare the accuracy of models according to the method of segmentation and mammographic views required, to establish the most time-efficient method whilst maintaining model accuracy.

METHODS AND MATERIALS

This is an ethically approved, hypothesis generating, retrospective, multicentre image analysis study (IRAS project ID: 266560). Consecutive CEM images were reviewed from two centres. At Site 1, images were acquired as part of ethically approved prospective imaging studies. CONTEST (ISRCTN12691785) is a study in which patients where there was high index of suspicion for cancer on clinical examination (P4-5) and/or ultrasound imaging (U4-5) had CEM performed prior to biopsy and CONDOR (researchregistry5895) a study which included females with biopsy-proven breast cancer. In the second study, images were acquired as part of routine clinical care for females over 40 years with a P4-5 examination and for younger females with suspicious ultrasound imaging (U4-5) or biopsy-proven malignancy without a recent standard mammogram. All CEM studies were performed prior to treatment. Details of image acquisition protocols and technical differences between the CEM systems are shown in Tables 1 and 2 respectively. Figure 1 illustrates a CEM study in the left CC position.

Table 2. Technical differences between CEM systems

CEM system	Mode	Low energy kV and target / filter[a]	High energy kV and target / filter[a]
GE Senographe Essential[16]	SenoBright	26 – 31kV Mo/Mo, Mo/Rh & Rh/Rh	45 – 49kV Mo/Cu or Rh/Cu
Hologic selenia dimensions[17]	I-View	25 – 33kV W/Rh & W/Ag	45 & 49kV W/Cu

CEM, contrast-enhanced mammography.
[a]Typical ranges covering 2–9 cm compressed breast thicknesses.

Inclusion criteria were as follows; females aged 18 years or older, mass lesion on CEM images—craniaocaudal (CC), mediolateral oblique (MLO) or both—with the corresponding pathology. Images with no abnormal enhancement or purely non-mass enhancement were excluded. Core biopsy results and final pathological diagnosis (where available), were retrieved from the patients records at the local site. In the case of multifocal or bilateral disease, all lesions with corresponding pathology were included.

Image segmentation

Image segmentation was performed on all RC images with a lesion present. Each lesion, on each view, was segmented using both a free-hand ROI (FH_ROI) and an ellipsoid ROI (ellipsoid_ROI). Both segmentation techniques were manually drawn by a radiologist with experience in breast imaging. The FH_ROI encompassed the entire lesion but did not extend beyond the lesion. Foreign bodies such as marker clips were carefully excluded from the ROI. The ellipsoid_ROI was drawn to cover the largest possible area of the lesion whilst excluding foreign bodies. The segmentation techniques are illustrated in Figure 2.

Table 1. Imaging protocols for CEM image acquisition

Site	CEM system	Contrast medium	Vol. of contrast	Flow rate	Time to imaging	Imaging duration	Order of image acquisition
1	Selenia Dimensions system (Hologic)	Omnipaque 300	1.5 mg/kg	2–3 ml/s automated	3 min	5 min	Index MLO Index CC Contralateral MLO Contralateral CC
2	Senographe Essential system (GE Healthcare)	Niopam 300	100 ml	3 ml/s automated	2 min	5 min	Variable

CC, craniocaudal; CEM, contrast-enhanced mammography; MLO, mediolateral oblique.

Figure 2. Segmentation of RC images of the right breast. Top row from left to right; 1a RCC, 1b RCC with FH_ROI, 1c RCC with ellipsoid_ROI. Bottom row from left to right; 2a RMLO, 2b RMLO with FH_ROI, 2c RMLO with ellipsoid_ROI. RC, recombined; ROI, region of interest.

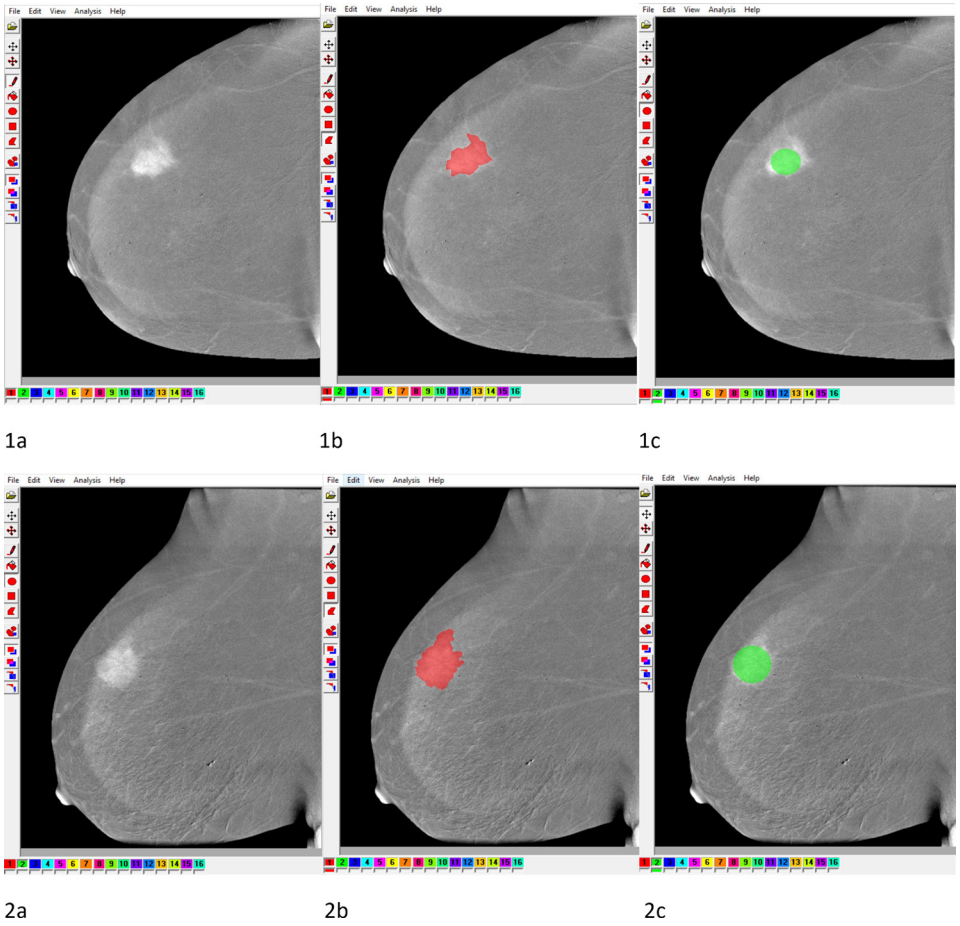

Textural analysis

Textural analysis was performed on raw DICOM images using MaZda analysis software.[18] Prior to conducting textural analysis, grey-normalisation and rebinning were conducted. Due to an absence of published data pertaining to textural analysis applied to CEM images at the time of study design, the model was proposed based on textural analysis work with breast MRI which demonstrated success using models based on grey length co-occurrence matrix (GLCM) textural data.[19,20] Textural features were extracted using first-order statistics based on histogram analysis (HIST) and GLCM. HIST features allowed quantification of the degree of enhancement, GLCM statistics were generated to assess lesion heterogeneity.[21] GLCM features are computed by defining both a direction (0°, 45°, 90°, 135°) and a distance between which the pixels are separated. As no directional variation in textural parameters is expected in breast imaging,[4] the output was averaged. Separation between pixel pairs was set at $n = 2$ for fine texture and $n = 5$ for coarse texture. This resulted in a combined total of 22 textural features.

Machine learning

Classification models were developed to categorise lesions as benign or malignant. Two different types of model, one according to type of ROI (Freehand *vs* ellipsoid) and the other according to mammographic view (CC *vs* MLO *vs* both) were considered. A training set where the final class labels were known was used to construct the classifier. A four-layered artificial neural network (ANN) classification algorithm, a technique based on a back-propagation learning method was employed.[22]

The input layer consisted of the 22 textural features generated from GLCM and HIST. Oversampling was performed to balance the class distribution at 2:1 (malignant:benign). Random samples for benign lesions were generated using a verified method, the synthetic minority oversampling technique (SMOTE).[23] New samples similar to input samples in the feature space were generated.The data were then split into training and test sets in a ratio of 75:25. Subset analysis was conducted using separate models to compare accuracy for:

(a) Type of ROI: FH_ROI *vs* ellipsoid_ROI
(b) Mammographic view: CC *vs* MLO *vs* combined (CC+MLO)

Statistical analysis

The results are shown by averaging the model accuracy over 30 runs. Diagnostic accuracy, sensitivity, specificity, positive-predictive value (PPV), negative-predictive value (NPV) and F1 score were calculated for each model. F1 score is a key measure of

Table 3. Histopathology of malignant lesions

Tumour subtype		
Ductal NST		220
Lobular		13
Mixed ductal/lobular		8
Tubular / tubular mixed		7
Medullary		1
Mixed ductal/mucinous		2
Mammary adenocarcinoma		2
Unavailable		2
Tumour grade		
1		25
2		112
3		98
Unavailable		20
Receptor status		
Oestrogen receptor		
	Positive	187
	Negative	56
	Unavailable	12
Progesterone receptor		
	Positive	160
	Negative	83
	Unavailable	12
HER-2 receptor		
	Positive	50
	Negative	190
	Unavailable	15

model accuracy for imbalanced data sets based on precision and recall relative to a specific positive class.[24]

Differences between models were assessed using a two-tailed independent sample means test for two models and ANOVA with Bonferroni correction. Coding analysis was performed using Python 3.7 on Jupyter notebooks. Effective sample size was not calculated as the work was primarily exploratory for hypothesis generation.

RESULTS

238 patients with a total of 269 enhancing mass lesions were included. Of these, 14 were benign and 255 were malignant, the imbalance of benign/malignant lesions was mitigated through oversampling. Histopathological details of the malignant lesions are shown in Table 3, and the benign lesions in Table 4.

Type of ROI

A total of 538 lesion views were included; all had textural features generated from both a FH_ROI and ellipsoid_ROI. Two models were developed based on the ROI-type. The relative accuracy of the two models is detailed in Table 5 below.

Table 4. Histopathology of benign lesions

Fibroadenoma	4
Chronic inflammation	2
Fat necrosis	1
Fibrocystic change	1
Benign granular cell tumour	1
Hamartoma	1
Papilloma without atypia	1
Benign phyllodes tumour	1
Unusual sclerosing lesion	1
Unknown/unspecified	1

Whilst the diagnostic accuracy of both models was greater than 0.9 which is deemed to be very good,[25,26] the ellipsoid_ROI model demonstrated significantly better results across all measures, including the F1 score ($p < 0.05$).

Mammographic view

All females had imaging performed in both CC and MLO positions. The majority of lesions, 255 (95%), were visible on both CC and MLO views, 8 (3%) were only visible on CC and 6 (2%) were only visible on MLO view. Textural features generated from both the FH_ROI and ellipsoid_ROI were included. Three models were developed based on the ROI-type; one using CC_ROI only, one using MLO_ROI only and a third using both CC_ROI and MLO_ROI. The relative accuracy of the three models alongside a comparison of accuracy calculated using one-way analysis of variance (ANOVA) is detailed in Table 6 below.

Whilst all three models demonstrate high levels of diagnostic accuracy (>0.94), significant differences were demonstrated between all measures other than AUC, which was consistently very high (>0.98). *Post-hoc* analysis on all other measures was conducted using multiple-comparison tests with Bonferroni correction, as shown in Table 7.

Overall, the model using both CC_ROI and MLO_ROI produced the most consistently good results across all measures. The CC_ROI model demonstrated a greater ability to detect benign lesions (higher specificity and NPV) whilst the MLO-ROI demonstrated a greater ability to detect malignant lesions (higher sensitivity and PPV) but overall accuracy and F1 score were lower.

DISCUSSION

The primary aim of this exploratory work was to establish whether radiomic modelling could be applied to CEM textural features derived from a multivendor data set to differentiate benign from malignant lesions. Subsequent to the inception of this project there has been a flurry of publications pertaining to textural analysis of CEM images.[7–13] However, this remains the first study to use a multivendor database, with a larger data set of lesions larger than

Table 5. ROI_model accuracy

ROI type	Accuracy (SD)	F1 score (SD)	AUC (SD)	Sensitivity (SD)	Specificity (SD)	PPV (SD)	NPV (SD)
FH	0.914 (0.013)	0.928 (0.01)	0.974 (0.006)	0.953 (0.028)	0.891 (0.013)	0.841 (0.016)	0.969 (0.016)
Ellipsoid	0.947 (0.009)	0.955 (0.007)	0.986 (0.004)	0.998 (0.005)	0.916 (0.014)	0.878 (0.018)	0.998 (0.003)

AUC, area under the curve; NPV, negative-predictive value; PPV, positive-predictive value; ROI, region of interest; SD, standard deviation.

those used in many published studies. Our models produce sensitivities of 94.2–99.8%, considerably higher than those for CEM in the aforemention meta-analysis of human reader studies, and comparable to that of MRI.

CEM is becoming more widespread in clinical practice, with national guidelines supporting its use in place of MRI for local staging.[27] However, a recent meta-analysis demonstrates that whilst CEM has a greater specificity and lower false-positive rate than MRI, it is inferior for identifying malignant lesions; sensitivity 91 *vs* 97% respectively.[15]

We anticipate decision-support tools may be developed to provide additional quantitative information to the reporting radiologist, with the goal of increasing sensitivity and mitigating the risk of increased false-negative results. To maximise the benefit of such a tool,it will be important for it to be practicable in a real-world setting. Ultimately, for optimal clinical use, a radiomics package would be available on PACS (Picture Archiving and Communication System) workstations to allow quantifiable data to be extracted and used in real-time reporting, irrespective of the machine on which the images were acquired or the precise imaging protocol used. Our findings suggest that this will be possible.

Furthermore, despite the pragmatic real-world nature of our images, our results exceed the accuracy of many of those in the published literature, as illustrated in Table 8.[7–13]

Five of these publications come from two groups: the Mayo Clinic, USA[9–11] and Istituto Tumori "Giovanni Paolo II", Italy.[7,8] Interestingly, despite the overlap of the CEM images from which the textural features were derived, substantial variation is seen in model accuracy measures. This may be related to different modelling techniques and emphasises the need for establishing basic technique and consistency.

For a radiomics tool to be clinically practical, it is important to minimise the additional time required to acquire the necessary information. This pertains both to the time taken for the images to be segmented and the time for the model to run. Therefore, unlike other studies that generated 100's or even 1000's of textural features, we built on existing work that demonstrated the importance of GLCM features of heterogeneity/entropy on breast MRI for differentiating benign from malignant lesions.[4,5]

Furthermore, previous studies—with the possible exception of Perek et al[12]—include textural feature data derived from both the LE and RC images. By contrast, our model only required feature data from RC images thereby reducing the radiologists workload—fewer images to segment—in addition to the required computing power with no loss in diagnostic accuracy.

We have sought to establish the best method of segmentation, by comparing the results of models built with data from free-hand or ellipsoid ROIs. To the best of our knowledge, this is the first study to address this question. Existing studies use a range of segmentation methods; including the whole tumour outline (equivalent of FH_ROI)[10] ; consistently sized rectangular_ROI either including the whole tumour and some surrounding tissue[7] or contained within the tumour—similar to ellipsoid_ROI[9] ; or sample patches around randomly selected pixels.[12] Whilst both ROI models in this study demonstrated high levels of accuracy, the ellipsoid_ROI demonstrated significantly better performance across all measures including the F1 score higher which is particularly reassuring due to the imbalanced data set. This may be especially useful for future modelling as segmenting using an

Table 6. Mammographic view model accuracy measures (ANOVA)

	Mammographic View			ANOVA	
	MLO	CC	Both	F	*p*
Accuracy (SD)	0.947 (0.015)	0.955 (0.011)	0.955 (0.006)	5.026	**0.009**
F1 score (SD)	0.959 (0.012)	0.964 (0.009)	0.966 (0.004)	4.855	**0.010**
AUC (SD)	0.985 (0.009)	0.988 (0.007)	0.987 (0.004)	1.438	0.243
Sensitivity (SD)	0.954 (0.029)	0.942 (0.009)	0.954 (0.011)	4.142	**0.019**
Specificity (SD)	0.944 (0.020)	0.962 (0.014)	0.956 (0.007)	12.287	**0.000**
PPV (SD)	0.904 (0.029)	0.935 (0.023)	0.915 (0.012)	14.683	**0.000**
NPV (SD)	0.974 (0.015)	0.966 (0.005)	0.977 (0.005)	3.266	**0.043**

AUC, area under the curve; NPV, negative-predictive value; PPV, positive-predictive value; ROI, region of interest; SD, standard deviation.

Table 7. *Post-hoc* direct comparison of mammographic view model accuracy measures

	Difference between mammographic views (*p*-value)		
	MLO *vs* CC	MLO *vs* Both	CC *vs* Both
Accuracy	<0.00001	<.00001	0.869
F1 score	<0.00001	<.00001	<.00001
Sensitivity	0.048	0.959	0.036
Specificity	0.020	0.024	0.457
PPV	0.001	0.036	0.025
NPV	0.035	0.089	0.029

AUC, area under the curve; CC, craniocaudal; MLO, mediolateral oblique;NPV, negative-predictive value; PPV, positive-predictive value; ROI, region of interest; SD, standard deviation.

ellipsoid ROI is substantially quicker than delineating the precise boundary of the lesion using a freehand technique. Future work is required to establish whether these findings can be applied to auto-segmentation techniques, thus further reducing the workload for the reporting radiologist.

A second novel aspect of this study is that we have investigated whether it is necessary to segment both mammographic MLO and CC views. The majority of previous studies have used data from both views,[9–12] two studies used whichever view the lesion was better seen on[7,8] and one used CC alone.[13] Our data suggest that whilst overall the model using ROIs on both imaging views produces a more accurate model; diagnostic accuracy remains high for models designed with single views alone, with no significant difference in AUC values across all three models. Of the models looking at single views alone, the CC_ROI model demonstrated higher diagnostic accuracy and F1 score and was more accurate at identifying benign lesions with higher specificity and PPV. The MLO_ROI model was better at detecting malignant lesions with a higher NPV and sensitivity. Although the differences between the single-view models and the two-view model are statistically significant, the additional time to draw the second ROI and compute the textural analysis figures needs to be considered. We suggest that the marginal gains, *e.g.* diagnostic accuracy of 0.947 *vs* 0.955 or F1 score of 0.959 *vs* 0.99 do not justify the additional time required for the two-view model. Furthermore, whilst the results suggest that the MLO model is preferable, if a lesion is only visible on CC, we propose that this should also be included. Future work to build a model using *either* CC or MLO views is recommended. Interestingly, the published models that have taken this approach do appear to have higher accuracy than those using both views or CC alone,[7,8,13] but due to wide variation in other methodological aspects of the studies, direct comparison is not feasible.

The main limitation of this study is the modest sample sizes which limits the validity of the modelling. In particular, the benign lesions subset was very small, requiring mitigation through oversampling techniques. Whilst the consistently high F1 score is reassuring and supports model accuracy and stability despite the imbalanced data set, further validation with a larger data set is required. In addition, all segmentation was conducted by the same reader. Whilst this prevents confounding due to inter-reader variability, it reduces the generalisability of the data modelling. It will be necessary to demonstrate reproducibility of segmentation with consideration of both inter- and intrareader variability in future work.

CONCLUSION

Our work suggests that it is only necessary to segment single view RC images using an ellipsoid_ROI to build an accurate model to discriminate benign and malignant lesions. We have shown that this technique can be applied to multivendor images acquired using differing imaging protocols. These findings will aid progress of CEM radiomics modelling towards a clinically applicable tool.

Table 8. Diagnostic accuracy measures of published studies

Paper	Model	Accuracy	AUC	Sensitivity	Specificity	PPV	NPV
Savaridas	-	0.955	0.988	0.954	0.962	0.878	0.998
Fanizzi[a]	-	0.875	0.931	0.875	0.917	NR	NR
Losurdo[a]	Embedded STAT	0.807	NR	0.864	0.750	NR	NR
	Wrapper STAT	0.809	NR	0.903	0.716	NR	NR
Patel[a]	-	0.90	0.95	0.88	0.92	NR	NR
Gao[a]	-	0.85	0.84	0.89	0.80	NR	NR
Danala[a]	RC	0.685	0.737	NR	NR	0.875	0.615
Perek	FT AlexNet	NR	0.843	NR	NR	NR	NR
	RawNet	NR	0.824	NR	NR	NR	NR
Lin	Rad-Score	NR	0.868	0.700	0.800	NR	NR

AUC, area under the curve; NPV, negative-predictive value; NR, not reported; PPV, positive-predictive value.
[a]Case overlap

ACKNOWLEDGEMENTS

We wish to thank Katherine Schofield, Lead Medical Physicist for NHS National Services Scotland for her knowledge regarding the technical differences between the CEM systems.

CONFLICT OF INTEREST

No conflict of interest to declare, true for all authors.

FUNDING

British Society of Breast Radiology grant, TENOVUS Scotland.

REFERENCES

1. Jochelson MS, Dershaw DD, Sung JS, Heerdt AS, Thornton C, Moskowitz CS, et al. Bilateral contrast-enhanced dual-energy digital mammography: feasibility and comparison with conventional digital mammography and MR imaging in women with known breast carcinoma. *Radiology* 2013; **266**: 743–51. https://doi.org/10.1148/radiol.12121084
2. Castellano G, Bonilha L, Li LM, Cendes F. Texture analysis of medical images. *Clin Radiol* 2004; **59**: 1061–69. https://doi.org/10.1016/j.crad.2004.07.008
3. van Timmeren JE, Cester D, Tanadini-Lang S, Alkadhi H, Baessler B. Radiomics in medical imaging-" how-to" guide and critical reflection. *Insights Imaging* 2020; **11**(1): 91. https://doi.org/10.1186/s13244-020-00887-2
4. Gibbs P, Turnbull LW. Textural analysis of contrast-enhanced Mr images of the breast. *Magn Reson Med* 2003; **50**: 92–98. https://doi.org/10.1002/mrm.10496
5. Wang Y, Liao X, Xiao F, Zhang H, Li J, Liao M. Magnetic resonance imaging texture analysis in differentiating benign and malignant breast lesions of breast imaging reporting and data system 4: a preliminary study. *J Comput Assist Tomogr* 2020; **44**: 83–89. https://doi.org/10.1097/RCT.0000000000000969
6. Davnall F, Yip CSP, Ljungqvist G, Selmi M, Ng F, Sanghera B, et al. Assessment of tumor heterogeneity: an emerging imaging tool for clinical practice? *Insights Imaging* 2012; **3**: 573–89. https://doi.org/10.1007/s13244-012-0196-6
7. Fanizzi A, Losurdo L, Basile TMA, Bellotti R, Bottigli U, Delogu P, et al. Fully automated support system for diagnosis of breast cancer in contrast-enhanced spectral mammography images. *J Clin Med* 2019; **8**(6): 891. https://doi.org/10.3390/jcm8060891
8. Losurdo L, Fanizzi A, Basile TMA, Bellotti R, Bottigli U, Dentamaro R, et al. Radiomics analysis on contrast-enhanced spectral mammography images for breast cancer diagnosis: a pilot study. *Entropy* 2019; **21**: 1110. https://doi.org/10.3390/e21111110
9. Patel BK, Ranjbar S, Wu T, Pockaj BA, Li J, Zhang N, et al. Computer-aided diagnosis of contrast-enhanced spectral mammography: a feasibility study. *Eur J Radiol* 2018; **98**: 207–13. https://doi.org/10.1016/j.ejrad.2017.11.024
10. Gao F, Wu T, Li J, Zheng B, Ruan L, Shang D, et al. SD-CNN: a shallow-deep CNN for improved breast cancer diagnosis. *Comput Med Imaging Graph* 2018; **70**: 53–62. https://doi.org/10.1016/j.compmedimag.2018.09.004
11. Danala G, Patel B, Aghaei F, Heidari M, Li J, Wu T, et al. Classification of breast masses using a computer-aided diagnosis scheme of contrast enhanced digital mammograms. *Ann Biomed Eng* 2018; **46**: 1419–31. https://doi.org/10.1007/s10439-018-2044-4
12. Perek S, Kiryati N, Zimmerman-Moreno G, Sklair-Levy M, Konen E, Mayer A. Classification of contrast-enhanced spectral mammography (CESM) images. *Int J Comput Assist Radiol Surg* 2019; **14**: 249–57. https://doi.org/10.1007/s11548-018-1876-6
13. Lin F, Wang Z, Zhang K, Yang P, Ma H, Shi Y, et al. Contrast-Enhanced spectral mammography-based radiomics nomogram for identifying benign and malignant breast lesions of sub-1 cm. *Front Oncol* 2020; **10**: 573630. https://doi.org/10.3389/fonc.2020.573630
14. Savaridas SL, Tennant SL. Quantifying lesion enhancement on contrast-enhanced mammography: a review of published data. *Clin Radiol* 2022; **77**: e313–20. https://doi.org/10.1016/j.crad.2021.12.010
15. Pötsch N, Vatteroni G, Clauser P, Helbich TH, Baltzer PAT. Contrast-Enhanced mammography versus contrast-enhanced breast MRI: a systematic review and meta-analysis. *Radiology* 2022; **305**: 94–103. https://doi.org/10.1148/radiol.212530
16. Mackenzie A, Tyler N, Kell M. Technical evaluation of contrast enhanced mammography functions of GE essential system. . National Co-Ordinating Centre for the Physics of Mammography2020.
17. Kelly M, Rai M, Mackenzie A. Technical evaluation of contrast enhanced mammography functions using Hologic I-View software. . National Co-ordinating Centre for the Physics of Mammography2020.
18. Szczypiński PM, Strzelecki M, Materka A, Klepaczko A. MaZda -- a software package for image texture analysis. *Comput Methods Programs Biomed* 2009; **94**: 66–76. https://doi.org/10.1016/j.cmpb.2008.08.005
19. Waugh SA, Purdie CA, Jordan LB, Vinnicombe S, Lerski RA, Martin P, et al. Magnetic resonance imaging texture analysis classification of primary breast cancer. *Eur Radiol* 2016; **26**: 322–30. https://doi.org/10.1007/s00330-015-3845-6
20. Henderson S, Purdie C, Michie C, Evans A, Lerski R, Johnston M, et al. Interim heterogeneity changes measured using entropy texture features on T2-weighted MRI at 3.0 T are associated with pathological response to neoadjuvant chemotherapy in primary breast cancer. *Eur Radiol* 2017; **27**: 4602–11. https://doi.org/10.1007/s00330-017-4850-8
21. Szczypinski PM, Strzelecki M, Materka A. *Mazda - a software for texture analysis*; 2007. , pp.245–49.
22. Desai M, Shah M. An anatomization on breast cancer detection and diagnosis employing multi-layer perceptron neural network (MLP) and convolutional neural network (CNN). *Clinical EHealth* 2021; **4**: 1–11. https://doi.org/10.1016/j.ceh.2020.11.002
23. Cahyana N, Khomsah S, Aribowo AS. Improving Imbalanced Dataset Classification Using Oversampling and Gradient Boosting. 5th International Conference on Science in Information Technology (ICSITech); Yogyakarta, Indonesia. ; 2019. https://doi.org/10.1109/ICSITech46713.2019.8987499
24. Jubair S, Alkhateeb A, Tabl AA, Rueda L, Ngom A. A novel approach to identify subtype-specific network biomarkers of breast cancer survivability. *Netw Model Anal Health Inform Bioinforma* 2020; **9**(1). https://doi.org/10.1007/s13721-020-00249-4
25. Tumuluru P, Lakshmi C, Sahaja T, Prazna R. A Review of Machine Learning Techniques for Breast Cancer Diagnosis in Medical

Applications. Third International conference on I-SMAC (IoT in Social, Mobile, Analytics and Cloud) (I-SMAC); Palladam, India. ; 2019. https://doi.org/10.1109/I-SMAC47947.2019.9032427

26. Yue W, Wang Z, Chen H, Payne A, Liu X. Machine learning with applications in breast cancer diagnosis and prognosis. *Designs* 2018; **2**: 13. https://doi.org/10.3390/designs2020013

27. Radiologists TRCo*Guidance on screening and symptomatic breast imaging*. 4th edn. London: Royal College of Radiologists; 2019.